

# The Ginger-shaped Asteroid 4179 Toutatis: New Observations from a Successful Flyby of Chang'e-2

Jiangchuan Huang<sup>1,3\*</sup>, Jianghui Ji<sup>2\*</sup>, Peijian Ye<sup>1</sup>, Xiaolei Wang<sup>4</sup>,  
 Jun Yan<sup>5</sup>, Linzhi Meng<sup>3</sup>, Su Wang<sup>2</sup>, Chunlai Li<sup>5</sup>,  
 Yuan Li<sup>6</sup>, Dong Qiao<sup>7</sup>, Wei Zhao<sup>8</sup>, Yuhui Zhao<sup>2</sup>, Tingxin Zhang<sup>1</sup>,  
 Peng Liu<sup>8</sup>, Yun Jiang<sup>2</sup>, Wei Rao<sup>3</sup>, Sheng Li<sup>9</sup>,  
 Changning Huang<sup>10</sup>, Wing-Huen Ip<sup>6,11</sup>, Shoucun Hu<sup>2</sup>, Menghua Zhu<sup>6</sup>,  
 Liangliang Yu<sup>2</sup>, Yongliao Zou<sup>5</sup>, Xianglong Tang<sup>8</sup>, Jianyang Li<sup>12</sup>,  
 Haibin Zhao<sup>2</sup>, Hao Huang<sup>3</sup>, Xiaojun Jiang<sup>5</sup>, & Jinming Bai<sup>13</sup>

<sup>1</sup>China Academy of Space Technology, Beijing 100094, China.

<sup>2</sup>Key Laboratory of Planetary Sciences, Purple Mountain Observatory, Chinese Academy of Sciences, Nanjing 210008, China.

<sup>3</sup>Institute of Space System Engineering, Beijing 100094, China.

<sup>4</sup>Beijing Institute of Control Engineering, Beijing 100190, China.

<sup>5</sup>National Astronomical Observatories, Chinese Academy of Sciences, Beijing 100012, China.

<sup>6</sup>Space Science Institute, Macau University of Science and Technology, Taipa, Macau.

<sup>7</sup>Beijing Institute of Technology, Beijing 100081, China.

<sup>8</sup>Harbin Institute of Technology, Harbin 150001, China.

<sup>9</sup>School of Electronic Engineering and Computer Science, Peking University, Beijing 100871, China.

<sup>10</sup>Beijing Institute Of Space Mechanics and Electricity, Beijing 100076, China.

<sup>11</sup>Institute of Astronomy, National Central University, Taoyuan, Taiwan.

<sup>12</sup>Planetary Science Institute, AZ 85719, USA.

<sup>13</sup>Yunnan Astronomical Observatory, Chinese Academy of Sciences, Kunming 650011, China.

\* The authors contribute equally to this work. To whom correspondence should be addressed. E-mail:jjjh@pmo.ac.cn

**On 13 December 2012, Chang'e-2 conducted a successful flyby of the near-Earth asteroid 4179 Toutatis at a closest distance of  $770 \pm 120$  meters from the asteroid's surface. The highest-resolution image, with a resolution of better than 3 meters, reveals new discoveries on the asteroid, e.g., a giant basin at the big end, a sharply perpendicular silhouette near the neck region, and direct evidence of boulders and regolith, which suggests that Toutatis may bear a rubble-pile structure. Toutatis' maximum physical length and width are  $(4.75 \times 1.95 \text{ km}) \pm 10\%$ , respectively, and the direction of the  $+z$  axis is estimated to be  $(250 \pm 5^\circ, 63 \pm 5^\circ)$  with respect to the J2000 ecliptic coordinate system. The bifurcated configuration is indicative of a contact binary origin for Toutatis, which is composed of two lobes (head and body). Chang'e-2 observations have significantly improved our understanding of the characteristics, formation, and evolution of asteroids in general.**

## **Introduction**

Chang'e-2, the second Chinese probe dedicated to the exploration of the Moon, was launched on 1 October 2010 at 10:59:57 UTC. After it accomplished its primary objective, an extended mission was designed for Chang'e-2 to travel to the Sun-Earth Lagrangian point (L2) and then to an asteroid. On 9 June 2011, Chang'e-2 departed its lunar orbit and headed directly to L2, where it arrived on 25 August 2011 and began to perform space-environment exploration. The asteroid's subsequent flyby mission remained under consideration, and eventually, asteroid 4179 Toutatis was selected as the primary target for the flyby after considering the leftover fuel of the spacecraft, the capability of the tracking and control network, and the fact that the asteroid's closest approach to Earth would occur on 12 December 2012. An undisclosed story is that Chang'e-2 was intentionally controlled to move near L2 for more than 230 days to favor

the Toutatis-flyby injection maneuvers. On 15 April 2012, Chang'e-2 left L2. On 1 June 2012, the spacecraft began its mission to Toutatis. Chang'e-2 implemented the flyby on 13 December 2012 at 8:29:58.7 UTC at a closest distance of  $770 \pm 120$  ( $3\sigma$ ) meters from Toutatis' surface at a high relative velocity of  $10.73 \text{ km s}^{-1}$ , with highest-resolution images of better than 3 meters per pixel<sup>1</sup>. As of 14 July 2013, Chang'e-2 is still traveling into outer space over 50 million kilometers away from Earth, and it is the first successful multiple-type-objective probe in history that has ever visited the Moon, a Lagrangian point, and an asteroid.

Asteroids are remnant building blocks of the formation of the Solar System. They provide key clues to understanding the process of planet formation, the environment of the early Solar nebula, and even the occurrence of life on Earth. Toutatis, as an Apollo near-Earth asteroid in an eccentric orbit that originates from the main belt, was a good target for Chang'e-2's flyby mission because this asteroid is full of fascinating puzzles. The 3-D shape of Toutatis has been well reconstructed, and its spin state has been determined, from extensive radar measurements taken at Arecibo and Goldstone<sup>2-9</sup> since 1992 during its closest approaches to Earth, once every four years. The results indicate that Toutatis is characterized as a non-principal-axis rotator; this tumbling asteroid rotates about its long axis with a period of 5.4 days, and the long-axis precession period is 7.4 days<sup>7</sup>; this precession may be induced by the Earth's tides during each close-in flyby<sup>10</sup> and the Yarkovsky-O'Keefe-Radzievskii-Paddack (YORP) effect<sup>11</sup>. Moreover, detailed geological features, such as complex linear structures and concavities, have been revealed in Hudson et al.'s model<sup>5</sup> at an average spatial resolution of  $\sim 34$  m. Hence, the primary issue of concern is whether the derived radar models accurately represent the real appearance of Toutatis. Furthermore, some features such as boulders and regolith on its surface have been speculated to exist in previous radar models<sup>5,6</sup>. It was hoped that this mystery could be solved by obtaining optical images during a spacecraft's close flyby. Furthermore, small asteroids at the km scale are believed to have a so-called rubble-pile structure, which means that they consist

of a loose collection of fragments under the influence of gravity. Therefore, the second major question arises — whether Toutatis is also an agglomeration of gravitationally bound chunks with such a fragile structure.

The optical images of Toutatis were obtained using one of the onboard engineering cameras, which were originally designed to monitor the deployment of solar panels on the spacecraft and to photograph other objects (such as the Earth and Moon) in space. The camera that is capable of color imaging has a lens with a focal length of 54 mm and a 1024-by-1024-pixel CMOS detector, and it has a field of view (FOV) of  $7.2^\circ$  by  $7.2^\circ$ . A solar panel shields the camera from sunlight to help minimize stray light. The FOV was partly occulted by the solar panel, and thus some of the images were cut off from the early gallery. As part of the imaging strategy, Chang'e-2 maneuvered to adjust the camera's optical axis to lie antiparallel to the direction of the relative velocity vector between the probe and Toutatis. Imaging during the inbound trajectory was not ideal because there was a large Sun-Toutatis-Chang'e-2 phase angle of  $\sim 143.6^\circ$ . Therefore, Chang'e-2 completed an attitude adjustment approximately an hour ahead of the flyby epoch to prepare for the outbound imaging. The overall imaging time was approximately 25 minutes, and the interval for each snapshot was 0.2 seconds. During the mission, the spacecraft collected more than 400 useful images totaling 4.5 GB of data. Figure 1 shows several outbound images of Toutatis. Panel e, which was the first panoramic image, was taken at a distance of  $\sim 67.7$  km at a resolution of  $\sim 8.30$  m (see Supplementary Figure 1), whereas panel a, which was the third in a sequence of images, corresponds to an imaging distance of  $\sim 18.3$  km at a local resolution of  $\sim 2.25$  m, as shown in Fig. 1. The present highest-resolution optical image has a resolution that is significantly finer than the 3.75 m resolution of the known radar model<sup>8,9</sup>, although the radar images cover nearly the entire surface of Toutatis, whereas the optical images cover only one side of Toutatis' surface.

## Results

We tested several methods to directly establish the 3-D model of Toutatis based on the optical images collected by Chang'e-2. However, there is no satisfactory outcome because of the narrow viewing angle and the local high-resolution images. Therefore, 3-D models developed based on delay-Doppler radar measurements<sup>5,8,9</sup> were adopted to discern the attitude of Toutatis in the approaching epoch.

Based on the attitude of the probe and its camera, the relative position between the asteroid and the probe, and optical images, in combination with the models of Hudson et al. and Busch et al.<sup>5,8,9</sup>, which were utilized to match the spin state of Toutatis (see Supplementary Figure 2), the direction of the principal axis was measured to be  $(250 \pm 5^\circ, 63 \pm 5^\circ)$  with respect to the J2000 ecliptic coordinate system<sup>5,12</sup>, and the fundamental parameters are summarized in Table 1. Our result is in good agreement with the previous prediction<sup>8</sup>, which indicates that Toutatis' spin status was greatly changed because of tidal interaction with the Earth during the 2004 flyby, which had a closest distance of  $\sim 0.01$  AU<sup>8,10</sup>. Furthermore, we again measured Toutatis' physical size from the images, and its maximum length and width were estimated to be  $(4.75 \times 1.95 \text{ km}) \pm 10\%$ , respectively (see Supplementary Section 3).

### New Geological Features from Chang'e-2 Observation

The shape of Toutatis resembles that of a ginger root (Fig. 1), where the bifurcated asteroid mainly consists of a head (small lobe) and a body (large lobe). The two major parts are not round in shape, and their surfaces have a number of large facets. In particular, at the end of the body, there appears to be a huge square concavity, which could be of large-impact origin. Regarding the asteroid's appearance, craters are more prominent on Toutatis than on Itokawa. In contrast, we clearly see fewer boulders on Toutatis, although many smaller blocks may have been missed because of the resolution of Chang'e-2 flyby images.

In comparison with the radar models<sup>3-5</sup>, the proximate observations from Chang'e-2's flyby have revealed several remarkable discoveries concerning Toutatis, among which the presence of the giant basin at the big end appears to be one of the most compelling geological features, and the sharply perpendicular silhouette in the neck region that connects the head and body is also quite novel. A large number of boulders and several short linear structures (Fig. 1) are also apparent on the surface, although the lack of sharp contact in the radar model may be an effect of the SHAPE software<sup>13</sup>.

## **Concavities**

The giant basin at the big end of Toutatis has a diameter of  $\sim 805$  m, and we surmise that one or more impactors may have collided with the asteroid in this region, thereby gouging out such an enormous basin. Judging by the contrast of its relatively subdued relief with large impact basins on other asteroids, Mathilde and Eros, this large-end depression may be attributable to the internal structure of the large lobe, with smaller impact features overlying it. The most significant feature is the ridge around the largest basin. The wall of this basin exhibits a relatively high density of lineaments, some of which seem to be concentric to the basin. There are also several linear structures outside the basin that are roughly parallel to the basin rim (Fig. 2a). These ridges are indicative of an internal structure on small bodies<sup>14,15</sup>. Most of the ridges near the largest basin at the big end are most likely related to the huge stress energy during impact. The interior material in the deep region would have been scattered across Toutatis' surface by the large impact that formed the basin, leading to the fracturing of the asteroid. Hence, one may speculate that the asteroid most likely has a rubble-pile internal structure.

More than fifty craters have been identified from the flyby images, and they have diameters ranging from 36 to 532 m (with an average of  $\sim 141$  m).  $\sim 44\%$  of the craters exceed 100 m in diameter, which is consistent with Hudson et al.'s model. From the close-up image, a crater

of high morphological integrity (with a diameter of  $\sim 62$  m) can be clearly observed, whereas tens of boulders (with lengths of  $\sim 20$ - $30$  m) are randomly distributed nearby (Fig. 2b). Two concavities are closely carved into the surface: the larger (with a diameter of  $\sim 368$  m) has a relatively vague outline, whereas the smaller (with a diameter of  $\sim 259$  m) has a relatively clear edge. Based on their appearance, we suspect that the relatively smaller, young crater (marked with the letter B) is superimposed on the larger, ancient crater (marked with the letter A) (Fig. 2a).

Although the images show that parts of the observed surface areas have a high degree of exposure, the topographical features of the craters were identified based on visual inspection and automatic annotation. Therefore, we identified craters on the large and small lobes individually, including vaguely shaped candidate craters on the highly exposed areas, for the investigation of the cumulative and relative size-frequency distributions (see Supplementary Section 4)<sup>16</sup>. Figure 3 indicates that the surfaces of the two lobes are very likely to share a similar cratering history because their relative size-frequency profiles for craters<sup>17</sup> look alike throughout a range of diameters. Furthermore, the craters on the two lobes are not in saturation equilibrium, as the two profiles do not tend toward stability with increasing crater diameter (Fig. 3a). An abundance of craters would suggest that Toutatis suffered from many impacts of interplanetary projectiles in the past.

## **Boulders**

From the flyby images, more than thirty boulders can be clearly discerned. They have lengths that range from 12 to 81 m, with an average of  $\sim 32$  m. Approximately 90% of the boulders are less than 50 m in diameter. The largest boulder, along with other large boulders, is located near the neck region (Fig. 2a). It is believed that a large ejected fragment is empirically associated with a large crater<sup>18,19</sup>. The boulders are suggested to be those non-escaping ejecta that re-

impact onto the asteroid's surface within a short timescale<sup>20</sup> . Recently, the Goldstone radar images of 12 December 2012 have also suggested that several 10-m-scale bright features may be boulders<sup>8</sup> . However, the optical images, although they were collected on only one side of the asteroid, have an advantage over the radar models<sup>5,8</sup> in uncovering local fine features on the surface of Toutatis.

## **Regolith**

Two craters in the neck area are indicative of the granular flows in the inner flanks. The upper regolith near the craters is fine grained, whereas the lower is relatively coarse, and very many fragments are present (Fig. 2a). Such a structure may indicate the redistribution of regolith via downslope or resurfacing processes, which may be related to the inclined terrain and the orientation of gravity<sup>20</sup> . The results are in good agreement with those of polarimetric observations<sup>21,22</sup> , thereby indicating that Toutatis is covered with fine regolith made up of light-transmitting materials. The same features have also been reported on Lutetia's surface<sup>23</sup> . Furthermore, the characteristics once again suggest that Toutatis' surface may consist of a fine granular or regolith layer with the porosity of lunar soils<sup>4</sup> . The latest results imply that this asteroid may bear an undifferentiated L-chondrite surface composition<sup>24</sup> .

There is additional evidence that supports the existence of regolith on Toutatis' surface. The average thermal inertia for Toutatis may have a low profile, according to an empirical relation between the thermal inertia and the effective diameter<sup>25</sup> . For a non-principal-axis rotator such as Toutatis, the global redistribution of regolith that results from lofting may also be one of the factors that contributes to the low surface thermal inertia<sup>25</sup> . A considerable number of mm-sized grains may constitute Toutatis' regolith (Fig. 2b), and the regolith depth on the surface might range from several centimeters to several meters. Clearly, Toutatis' thermal inertia seems to be much less than that of Itokawa<sup>26</sup> ; thus, the terrain of Toutatis is a bit smoother than that



of Itokawa, and the boulders on Toutatis' surface are less numerous than those on Itokawa's surface, which is mostly embedded with numerous pebbles and gravel in all regions.

## **Linear Structures**

Several types of linear structures, which are primarily composed of troughs and ridges that appear to be common for small asteroids<sup>27,28</sup>, can be easily observed on Toutatis' surface. Notable linear structures are apparent in the radar models<sup>5</sup>; however, the flyby images do not identify any linear features that have been previously reported because the relevant part of the surface was invisible to Chang'e-2. The present linear structures, which are similar to the short linear structures of Itokawa, are clearly observed<sup>29</sup> to have a length of 120-330 m in the visible regions of the images. The troughs, which are similar in appearance to groove-like features, are primarily scattered over the small lobe; they have an average length of  $\sim 170$  m, and they are approximately orientated along the long axis of the asteroid (Fig. 2a). Generally, troughs are related to extensions resulting from tensile stress in the plane of the surface<sup>15</sup>. Consequently, they may be produced by the tensile stresses that arise from nearby impact cratering or other geological processes.

## **Discussion**

As mentioned above, the existence of the giant basin and its surroundings provides direct evidence that Toutatis is likely to be a rubble-pile asteroid. In this case, the asteroid could re-assemble itself into a weak aggregate of large fragments via a heavy impact or many smaller impacts; in this manner, the large interior voids could absorb the collision energy and further resist huge collisions in the formation process. Furthermore, a vast majority of S-type asteroids appear to possess rubble-pile structures with an average porosity of  $\sim 15\% - 25\%$ <sup>30</sup>. Recent investigations have demonstrated that the typical bulk density of L ordinary chondrites is  $\sim 3.34$

$\text{g cm}^{-3}$  <sup>24,30</sup> . Assuming a density of  $2.1 - 2.5 \text{ g cm}^{-3}$  <sup>20</sup> , Toutatis may have a porosity in the range  $\sim 25\%$  to  $\sim 37\%$ , thereby implying that it may be an intermediate body between Eros ( $\sim 20\%$ <sup>30</sup>) and Itokawa ( $\sim 41\%$ <sup>26</sup>) with respect to surface features. Moreover, strong evidence from N-body simulations indicates that two km-sized objects with rubble-pile structures would produce Toutatis-like objects<sup>31</sup> . In summary, we may conclude that Toutatis is not a monolith but most likely a coalescence of shattered fragments.

The bifurcated configuration means that Toutatis is comprised of two major lobes, similar to Itokawa, thereby implying that Toutatis is a contact binary, which is an asteroid type that may constitute more than 9% of the NEA population. Km-sized contact binaries, such as 4486 Mithra and 4769 Castalia, share an irregular, significantly bifurcated shape<sup>32</sup> . The following question then arises: how do these contact binaries form?

Several formation mechanisms have been proposed to produce such bifurcated configurations. The first scenario supposes that the two major lobes were two separate objects, which were moving at a sufficiently low relative speed to yield a contact binary<sup>26</sup> . The difference in the orientations of head and body may be indicative of their diverse origins and further suggests that the two parts were once detached. The second scenario includes the YORP and binary YORP (BYORP) effects, which are likely to form contact binaries<sup>33</sup> , especially for those objects with slow rotational periods. In this scenario, two components, which may be major fragments of a parent body, suffer re-impact and recombination, thereby leading to the formation of a bifurcated configuration. The third scenario suggests that catastrophic collisions may have gouged out the giant basin and a number of craters on Toutatis' surface. The boulders near three potential arc depression terrains (Figure 2a) imply that the head may have experienced severe impacts. Last but not least, tidal disruption from a close encounter with a terrestrial planet is also likely to play a role in the formation of such a contact binary. In short, the above-mentioned scenarios may have actually occurred during Toutatis' history. Hence, we infer that

Toutatis may be a reconstituted contact binary.

The Chang'e-2 flyby has revealed several new discoveries regarding Toutatis, e.g., the giant basin at the big end, the sharply perpendicular profile about the neck region, and direct images of distributed boulders and surface regolith. It is the first time that geological features on Toutatis' surface have been observed so clearly. All these observations suggest that Toutatis may bear a rubble-pile structure, similar to other S-type asteroids, such as Itokawa. Moreover, the close-up imaging results for the asteroid provide further indication that the bifurcated configuration that is related to the formation of contact binaries appears to be quite common among the NEA population. The observations of Chang'e-2 have significantly improved our understanding of the formation and evolution of these building blocks of the Solar System.

## Methods

To adapt to Chang'e-2's characteristics of high control accuracy and the wide FOV of  $7.2^\circ$  by  $7.2^\circ$  of the engineering camera, a close-approach strategy and a specific imaging design were developed. As shown in Supplementary Figure 1,  $L$ ,  $S$ , and  $\Delta t$  represent the minimum distance of rendezvous, the imaging distance, and the time interval between two sequential images, respectively. The camera optical axis pointed in the direction of the relative velocity between the probe and Toutatis, which remained nearly unchanged during the flyby. After a short time at the closest approach, the camera captured Toutatis; the asteroid was contained in the FOV, but the imaging size decreased as the departure distance increased. By solving the geometric relation between Image 2 and Image 3, the distances  $L$  and  $S$  and the resolution of each image were determined for the Chang'e-2 observations.

Taking into account the various characteristics of the specific approach design and imaging strategy for the flyby, a physical size of  $(4.75 \times 1.95 \text{ km}) \pm 10\%$  for the illuminated region of the asteroid surface was statistically estimated from the sequence of images recorded by the

CMOS detector during the flyby. The determined size is in good agreement with that of the radar model<sup>5</sup> (see Supplementary Sections 1 and 3).

The attitude of a rigid body in space is determined by its rotations around three axes of an orthogonal coordinate system. To define the attitude of Toutatis in each optical image (Supplementary Figure 2a), the three axes  $l_1$ ,  $l_2$ , and  $l_3$  are defined as follows:  $l_1$  and  $l_2$  extend through Toutatis' centroid in the images along the directions of the long axis and short axis, respectively, and are perpendicular to each other.  $l_3$  is perpendicular to the imaging plane and constitutes a right-handed coordinate system with  $l_1$  and  $l_2$ .

To match its shape to the optical images, we rotated the model of Busch et al. in intervals of  $5^\circ$  for each Euler angle around the three axes of the body-fixed coordinate system in space. Next, we chose three criteria of the orientation of the asteroid's long-axis, the ratio of length to width, and the obvious topographical feature at the joint of the two lobes of Toutatis — to ensure that the radar model agreed with the optical images from Chang'e-2, as shown in Supplementary Figure 2a. The most approximate attitude was finally obtained by rotating the radar model and comparing it with the optical image, as shown in Supplementary Figure 2b. The coordinate transformation from the asteroid's body-fixed system to the J2000.0 equatorial coordinate system were expressed in terms of three components of Euler angles. The directions of the principal axes were then obtained according to the attitude of the radar model.

The craters and other geological features were identified via both visual inspection and automatic annotation. In this case, dozens of low-lying regions were noted, and their positions, contours, and sizes were obtained using surface-structure-analysis techniques. The feature points on the edge of each crater were labeled manually based on the treatment of the imaging process and the radar model. After the points were marked, a piecewise-quadratic curve was fitted to them, and closed curves were obtained as contour profile. The sizes of the craters (and boulders) were calculated based on the resolution for each image and the fitted contour profiles.

## References

- [1] Huang, J. C. et al. The engineering parameters analysis of (4179) Toutatis flyby mission of Chang'e-2. *Science China Technological Sciences* **43**, 596-601 (2013).
- [2] Hudson, R. S. & Ostro, S. J. Shape and non-principal axis spin state of Asteroid 4179 Toutatis. *Science* **270**, 84-86 (1995).
- [3] Ostro, S. J. et al. Radar images of Asteroid 4179 Toutatis. *Science* **270**, 80-83 (1995).
- [4] Ostro, S. J. et al. Asteroid 4179 Toutatis: 1996 radar observations. *Icarus* **137**, 122-139 (1999).
- [5] Hudson, R. S., Ostro, S. J. & Scheeres, D. J. High-resolution model of Asteroid 4179 Toutatis. *Icarus* **161**, 346-355 (2003).
- [6] Busch, M. W. et al. Determining asteroid spin states using radar speckles. *Icarus* **209**, 535-541 (2010).
- [7] Busch, M. W. et al. Twenty years of Toutatis. *EPSC-DPS2011* **6**, 297 (2011).
- [8] Busch, M. W. et al. Internal structure of 4179 Toutatis. 2012 AGU Fall Meeting, P31A-1873 (2012).
- [9] Takahashi, Y., Busch, M. W. & Scheeres, D. J. Spin State and Moment of Inertia Characterization of 4179 Toutatis, *AJ* **146**, 95 (2013).
- [10] Scheeres, D. J. Rotational fission of contact binary asteroids. *Icarus* **189**, 370-385 (2007).
- [11] Bottke, W. F., Vokrouhlicky, D., Rubincam, D. P. & Broz, M. in *Asteroids III* (eds. Bottke, W. F. et al.)(Univ. of Arizona Press, Tucson, 2002).

- [12] Scheeres D. J., Ostro S. J., Werner R A, et al. Effects of gravitational interactions on asteroid spin states. *Icarus* **147**, 106-118 (2000).
- [13] Magri, C. et al. Radar observations and a physical model of Asteroid 1580 Betulia *Icaurs* **186**, 152-177 (2007)
- [14] Prockter, L. et al. Surface expressions of structural features on Eros. *Icarus* **155**, 75-93 (2002).
- [15] Thomas, N. et al. The geomorphology of (21) Lutetia: Results from the OSIRIS imaging system onboard ESA's Rosetta spacecraft. *Planet. Space Sci.* **66**, 96-124 (2012).
- [16] Zou, X.D. et al. Preliminary analysis of the 4179 Toutatis snapshots of the Chang'e-2 fly-by. *Icarus*, in press (2013).
- [17] Arvidson, R. E. et al. Standard techniques for presentation and analysis of crater size-frequency data. *Icarus* **37**, 467-474 (1979).
- [18] Gault, D. E., Shoemaker, E. M. & Moore, H. J. Spray ejected from the lunar surface by meteoroid impact. NASA Technical Document TND-1767, 1-39 (1963).
- [19] Thomas, P. C., Veverka, J., Robinson, M. S. & Murchie, S. Shoemaker crater as the source of most ejecta blocks on the asteroid 433 Eros. *Nature* **413**, 394-396 (2001).
- [20] Scheeres, D. J., Ostro, S. J., Hudson, R. S., DeJong, E. M. & Suzuki, S. Dynamics of orbits close to Asteroid 4179 Toutatis. *Icarus* **132**, 53-79 (1998).
- [21] Mukai, T. et al. Polarimetric observations of 4179 Toutatis in 1992/1993. *Icarus* **127**, 452-460 (1997).

- [22] Hudson, R. S. & Ostro, S. J. Photometric properties of Asteroid 4179 Toutatis from lightcurves and a radar-derived physical model. *Icarus* **135**, 451-457 (1998).
- [23] Vincent, J. B., Besse, S., Marchi, S., Sierks, H. & Massironi, M. Physical properties of craters on asteroid (21) Lutetia. *Planet. Space Sci.* **66**, 79-86 (2012).
- [24] Reddy, V. et al. Composition of near-Earth Asteroid (4179) Toutatis. *Icarus* **221**, 1177-1179 (2012).
- [25] Delbo', M., dell'Oro, A., Harris, A. W., Mottola, S. & Mueller, M. Thermal inertia of near-Earth asteroids and implications for the magnitude of the Yarkovsky effect. *Icarus* **190**, 236-249 (2007).
- [26] Fujiwara, A. et al. The rubble-pile asteroid Itokawa as observed by Hayabusa. *Science* **312**, 1330-1334 (2006).
- [27] Thomas, P. C. & Prockter, L. M. in *Planetary Tectonics*(eds. Watters, T. R & Schultz, R. A.) (Cambridge University Press, New York, 2010).
- [28] Robinson, M. S., Thomas, P. C., Veverka, J., Murchie, S. L. & Wilcox, B. B. The geology of 433 Eros. *Meteorit. Planet. Sci.* **37**, 1651-1684 (2002).
- [29] Demura, H. et al. Pole and global shape of 25143 Itokawa. *Science* **312**, 1347-1349 (2006).
- [30] Britt, D. T., Yeomans, D., Housen, K. & Consolmagno, G. in *Asteroids III*(eds. Bottke, W. F., Cellino, A., Paolicchi, P., & Binzel, R. P.)(Univ. of Arizona Press, Tucson, 2002).
- [31] Richardson, D. C., Leinhardt, Z. M., Melosh, H. J., Bottke, W. F. Jr. & Asphaug, E. in *Asteroids III*(eds. Bottke, W. F., Cellino, A., Paolicchi, P., & Binzel, R. P.)(Univ. of Arizona Press, Tucson, 2002).

- [32] Benner, L. A. M. et al. Near-Earth Asteroid 2005 CR37: radar images and photometry of a candidate contact binary. *Icarus* **182**, 474-481 (2005).
- [33] Steinberg, E. & Sari, R. Binary YORP effect and evolution of binary asteroids. *AJ* **141**, 55 (2011).
- [34] Krivova, N. V., Yagudina, E. I., & Shor, V. A. The orbit determination of (4179) Toutatis from optical and radar data. *Planet. Space Sci.* **42**, 741-745 (1994).
- [35] Milani, A., & Gronchi, G. Theory of orbit determination. (Cambridge University Press, Cambridge, UK, 2010).

**Supplementary Information** is available in the online version of the paper.

**Acknowledgements** The authors thank Michael W. Busch for his constructive comments that greatly helped to improve the original content of this manuscript. We thank the whole Chang'e-2 team to make the mission a success. We appreciate B. Yang for target observations before the flyby mission. We are grateful to R.P. Butler for English improvement of this manuscript. This research was supported by National Science and Technology Major Project, National Natural Science Foundation of China, the Innovative and Interdisciplinary program by CAS, and Key Laboratory of Planetary Sciences (2013DP173302), CAS. JYL's contribution to this work is not supported by any funds.



**Authors Contributions** J. C. H. was the leader of the asteroid mission. J. H. J. wrote the manuscript with contributions from other co-authors. J.C.H., P.J.Y. and T.X.Z. were responsible for the overall project design of the flyby mission to Toutatis, imaging strategy, and proposed the method of fundamental parameter analysis. H.B.Z., J.H.J., S.C.H., S.W., Y.H.Z., Y.J. and L.L.Y. contributed to ground-based observation, refined the trajectory solution for Toutatis, completed data analysis, prepared for figures and wrote the manuscript. L.Z.M, H.H. and W.R. took charge of overall design of probe system and data analysis. X.L.W. was responsible for controlling the attitude and the spacecraft's orbit, and contributed to the engineering parameters analysis. J.Y., C.L.L., Y.L.Z. and X.J.J. took charge of data collection, data pretreatment and the ground-based observation. Y.L. and M.H.Z. partly contributed to contents and prepared for figure. D.Q. contributed to the target selection and the design of transfer orbit. W.Z., P.L. and X.L.T. were in charge of the algorithm of optical images and obtained the image information. S.L. was responsible for imaging process. C.N.H. developed the optical camera and determined the parameters of the camera. W.H.I and J.Y.L. contributed ideas and discussions in preparation for the manuscript. J.M.B. partly participated in the target observation. All authors contributed to the manuscript.

**Authors information** The authors declare no competing financial interests. To whom correspondence should be addressed. E-mail:jjjh@pmo.ac.cn.

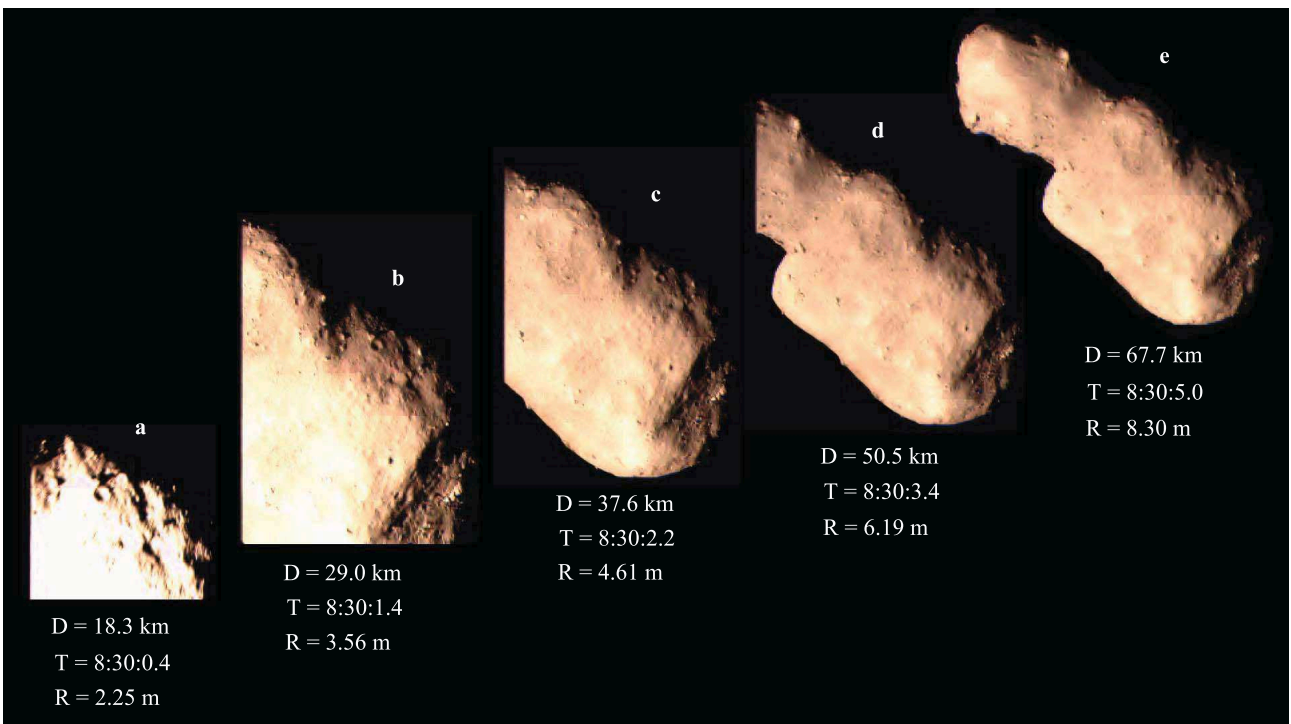


**Figure 1 | Outbound images of Toutatis acquired on 13 December, 2012 during Chang'e-2 flyby, indicative of the spacecraft being away from the asteroid (from a to e).** The left side of Toutatis is blocked by the solar panel in images a-d. The imaging distance (D), epoch of flyby (T, UTC) and resolution of each image (R) are shown for each snapshot, where the distance error for a is 1.1 km. The resolution of each image is linear with the distance.

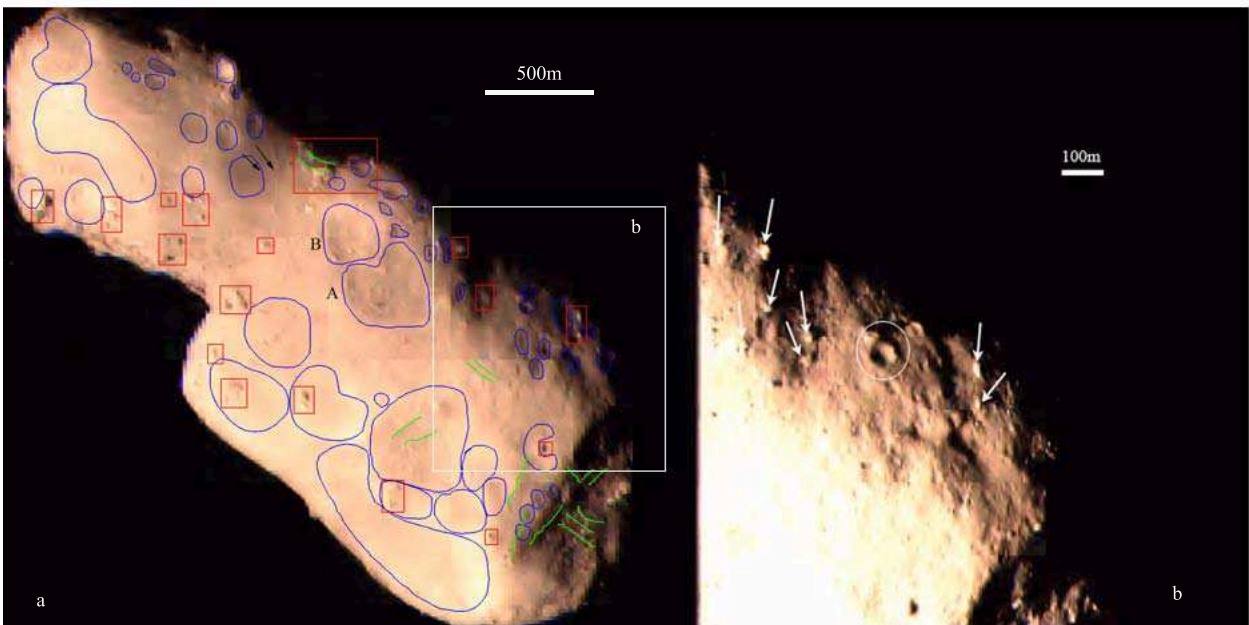


**Figure 2 |All kinds of geological features on the Toutatis' surface. (a)** All craters (blue profiles) and boulders (red squares) are outlined in the panoramic image of Toutatis. Two craters are closely distributed: the smaller crater (B) seemed to superimpose on the larger one (A). Green lines indicate the lineaments. Black arrows point the flow direction of the fine-grained regolith. **(b)** The enlarged portion shown (white box) in the left panel (a). A morphological-integrity crater can be observed. Tens of boulders are randomly distributed around.

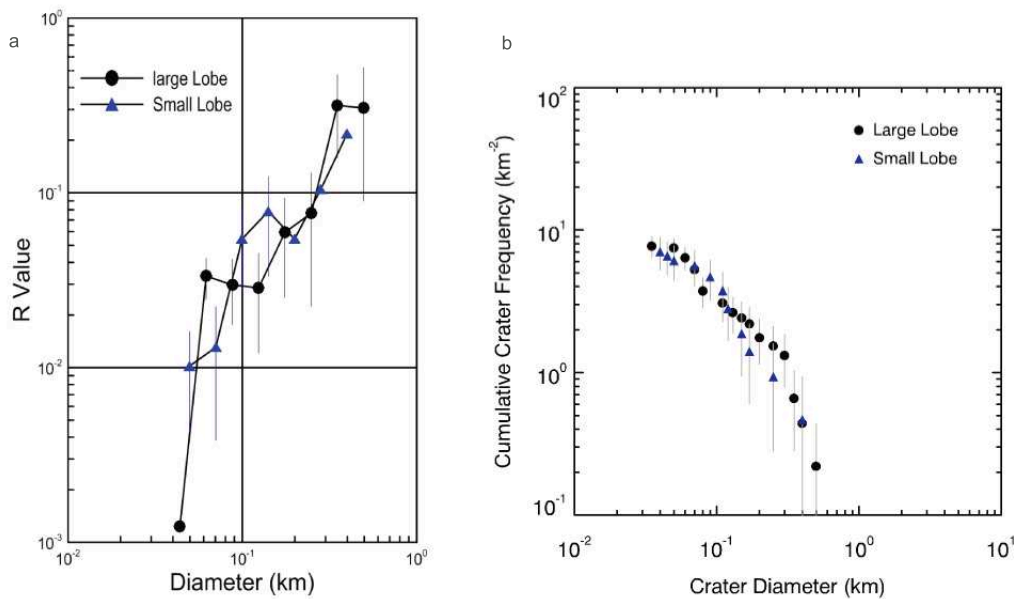


**Figure 3** |(a)The relative size-frequency distribution for craters on Toutatis. (b) The cumulative size-frequency distribution for craters on Toutatis. In panel (a) R plot was devised by the Crater Analysis Techniques Working Group<sup>17</sup> to better show the size distribution of craters and crater number densities for determining relative ages. The vertical position of the curve is a measure of crater density or relative age on the Toutatis: the higher the vertical position, the higher the crater density and the older the surface. In panel (b)  $x$ -axis stands for the crater diameter and  $y$ -axis represents the crater number larger than corresponding diameter on the investigated area. CSFD would easily inform that the size of craters distribute as diameters increase.

**Table 1. Parameters for Toutatis.**

Property	Value
Osculating Orbital elements	$a=2.5336$ AU, $e=0.6301$ $i=0.4466^\circ$ , $\Omega=124.3991^\circ$ $\omega=278.6910^\circ$ , $M=6.7634^\circ$
Special type	S (IV) <sup>5</sup>
Size (diameter) Major axes	$(x=4.60\pm 0.10$ km, $y=2.29\pm 0.10$ km, $z=1.92\pm 0.10$ km) <sup>5</sup> $(x=4.46\pm 0.10$ km, $y=2.27\pm 0.10$ km, $z=1.88\pm 0.10$ km) <sup>9</sup>
Rotational properties	
Rotation	5.4 day <sup>2,5</sup>
Precession	7.4 day <sup>2,5</sup>
Pole position in the space	$\beta = 250 \pm 5^\circ$ , $\lambda = 63 \pm 5^\circ$ $\beta = 54.6^\circ$ , $\lambda = 60.6^\circ$ <sup>8,9</sup> $\alpha = 258 \pm 5^\circ$ , $\delta = 40 \pm 5^\circ$
Density	2.5 g cm <sup>-3</sup> <sup>20</sup>

Using the data released by the Minor Planet Center<sup>34,35</sup> and optical data from the ground-based observational campaign sponsored by the Chinese Academy of Sciences, we determined Toutatis' orbit with uncertainties on the order of several kilometers. Osculating orbital elements were calculated for the flyby epoch of 13 December 2012 at 8:30 UTC, where  $a$ ,  $e$ ,  $i$ ,  $\Omega$ ,  $\omega$ , and  $M$  are the semi-major axis, the eccentricity, the inclination, the longitude of the ascending node, the argument of perihelion, and the mean anomaly, respectively.  $\beta$ ,  $\lambda$  and  $\alpha$ ,  $\delta$  are the longitudes and latitudes of the long axis of the asteroid in the J2000.0 ecliptic and equatorial coordinate systems, respectively.